Roll vortices induce new particle formation bursts in the planetary boundary layer

Janne Lampilahti[1], Hanna Elina Manninen[2], Katri Leino[1], Riikka Väänänen[1], Antti Manninen[3], Stephany Buenrostro Mazon[1], Tuomo Nieminen[1], Matti Leskinen[1], Joonas Enroth[1], Marja Bister[1], Sergej Zilitinkevich[1,3,4], Juha Kangasluoma[1,5], Heikki Järvinen[1], Veli-Matti Kerminen[1], Tuukka Petäjä[1,6], Markku Kulmala[1,5,6]

[1]Institute for Atmospheric and Earth System Research/Physics, Faculty of Science, University of Helsinki, Helsinki, Finland
[2]CERN, CH-1211 Geneva, Switzerland.
[3]Finnish Meteorological Institute, Helsinki, Finland.
[4]Department of Radio-physics, University of Nizhny, Novgorod, Russia.
[5]Aerosol and Haze Laboratory, Beijing Advanced Innovation Center for Soft Matter Science and Engineering, Beijing University of Chemical Technology, Beijing, China.
[6]Joint International Research Laboratory of Atmospheric and Earth System Sciences, Nanjing University, Nanjing, China.

Correspondence to: Janne Lampilahti (janne.lampilahti@helsinki.fi)

Abstract. Recent studies have shown the importance of new particle formation (NPF) to global cloud condensation nuclei (CCN) production, as well as to air pollution in megacities. In addition to the necessary presence of low-volatility vapors that can form the new aerosol particles, both numerical and observational studies have shown that the dynamics of the planetary boundary layer (BL) plays an important role in NPF. Evidence from field observations suggests that roll vortices might be favorable for inducing NPF in a convective BL. However, direct observations and estimates on the potential importance of this phenomenon to the production of new aerosol particles are lacking. Here we show that rolls frequently induce NPF bursts along the horizontal circulations, and that the small clusters and particles originating from these localized bursts grow in size similar to particles typically ascribed to atmospheric NPF that occurs almost homogeneously at a regional scale. We outline a method to identify roll-induced NPF from measurements and, based on the collected data, estimate the impact of roll vortices on the overall aerosol particle production due to NPF at a boreal forest site (83±34% and 26±8% overall enhancement in particle formation for 3-nm and 10-nm particles respectively). We conclude that the formation of roll vortices should be taken into account when estimating particle number budgets in the atmospheric BL.

1 Introduction

Atmospheric new particle formation (NPF) is a globally important source of aerosol particles and cloud condensation nuclei (CCN) (Dunne et al., 2016; Gordon et al., 2017; Kerminen et al., 2018; Kulmala et al., 2004), having potentially large influences on climate via aerosol-cloud interactions (Boucher et al., 2013) as well as on human health by increasing ultrafine particle number concentrations. NPF involves the formation of molecular clusters (~1.5 nm) in the atmosphere, and under specific conditions these clusters may grow to larger aerosol particles in the sub-100 nm size range. Under atmospheric

background conditions, increased concentrations of nucleation mode (sub-25 nm) particles likely come from recent NPF. When the particles are larger than ~50 nm in diameter they can act as nuclei for cloud droplets (Kerminen et al., 2012) and influence radiative and other properties of clouds (e.g. Gryspeerdt et al., 2014; Rosenfeld et al., 2014).

Numerical studies have shown that fluctuations in ambient temperature and relative humidity, caused by for example small-scale turbulence, large eddies such as roll vortices (Easter and Peters, 1994), or mixing over a temperature inversion (Nilsson and Kulmala, 1998) can lead to significant enhancements in new particle formation rate compared to only mean conditions. This is because the formation rate has a non-linear dependence on temperature and the gas-phase concentrations of the precursor vapors. Therefore, fluctuations in these variables, as opposed to mean conditions where the fluctuations are averaged out, can have a net enhancing effect on the source strength of aerosol particles by NPF.

In observational studies, increased nucleation mode particle concentrations have been measured in atmospheric layers where turbulent fluctuations were enhanced. For example in turbulent layers inside the residual layer (Wehner et al., 2010) and in the inversion capping a shallow mixed layer (Platis et al., 2015; Siebert et al., 2004). Other airborne measurements have found that during NPF the number concentration of nucleation mode particles shows considerable, up to an order of magnitude, variation within the BL (Crumeyrolle et al., 2010; Leino et al., 2019; O'Dowd et al., 2009; Schobesberger et al., 2013; Väänänen et al., 2016). One possible reason for this could be the effect of BL dynamics.

Convection in the BL often organizes into counter-rotating horizontal roll vortices or rolls that extend to the top of the BL (Figure 1, e.g. Atkinson and Wu Zhang, 1996; Etling and Brown, 1993; Young et al., 2002). Buzorius et al. (2001) and Nilsson et al. (2001) noted that roll vortices commonly occurred during NPF events and suggested that they might be especially conducive to NPF.

For example, in the boreal forest the vegetation is an important source of volatile organic compounds that can be oxidized into low-volatile organic vapors (Ehn et al., 2014). Due to higher wind speeds the shear-generation of turbulence close to the vegetation is stronger in rolls than in cellular type convection (Zilitinkevich et al., 2006). Therefore, roll updrafts are particularly efficient at transporting vapors and molecular clusters from the surface to the top of the BL. On top of the BL decreased temperature, turbulence and mixing over the inversion layer can lead to a supersaturation of the vapors and activation of the clusters, leading to subsequent NPF (Easter and Peters, 1994; Nilsson and Kulmala, 1998). The newly-formed particles grow in size in the weaker and wider downdraft and end up close to the surface where they may be deposited on surfaces or continue growing while being transported in the air. These

processes are illustrated in (Figure 2). The period for this sequence of processes is roughly an hour (Easter and Peters, 1994).

However direct observations of the effects of roll vortices on NPF are lacking. In this study we have analyzed co-located airborne and ground-based measurements from southern Finland during 2013-2015 in order to determine the effect of roll vortices on NPF.

2 Methods

We analyzed data from airborne measurement campaigns conducted between 2013-2015 in southern Finland (see Table 1 for a summary of the airborne campaigns). These measurements had a general goal of measuring the vertical and horizontal distribution of aerosol particles in the lower atmosphere over a rural boreal forest area, with a special emphasis on NPF. The airborne observations were complemented by the continuous and comprehensive aerosol measurements at the SMEAR II station (Hari and Kulmala, 2005). The main tool to detect roll vortices was a nearby weather radar. Also wind data from the airborne and ground-based measurements was used.

2.1 Zeppelin measurements.

In May-June 2013, in the framework of the PEGASOS (Pan-European Gas-AeroSOls Climate Interaction Study) project, aerosol particle and gas phase measurements were performed over Hyytiälä and Jämi in southern Finland using an instrumented Zeppelin NT (Neue Technologie) airship.

Here we analyzed measurements from the onboard neutral cluster and air ion spectrometer (NAIS) (Mirme et al., 2010; Mirme and Mirme, 2013) on May 8, 2013. The NAIS measured the particle number-size distribution in the diameter range 2-42 nm and ion number-size distribution in the diameter range 0.8-42 nm at 4 min time resolution. We used the total particle data from the positive polarity of the instrument.

During the measurement the inlet of the NAIS was pushed out from the window of the zeppelin's gondola. The data was corrected for diffusional losses in the one meter long, 37 mm inner diameter, inlet tube (Gormley and Kennedy, 1948) and converted to standard conditions (293.15 K and 1 atm) using Equation 1, which can be derived using the ideal gas law:

$$N_{std} = \left(\frac{1\,\mathrm{atm} \times T}{293.15\,\mathrm{K} \times p} \right) \times N \qquad (1)$$

where N refers to number concentration, T to temperature and p to pressure. The temperature and pressure recorded by the instrument were used in the corrections. Any losses occurring at the inlet nozzle were assumed to be negligible due small size of the measured particles and relatively low airspeed, so that the particles closely followed streamlines.

The zeppelin measurements consisted of consecutive profiles. Each profile was a slow and even ascend (~25 min) from ~100 m up to ~1 km above ground followed by a fast descend (~5 min) while the speed relative to the surrounding air (airspeed) was kept at ~20 m/s. The vertical profiles were flown over the same circular area that was only ~4 km in diameter (see Figure 3). The flights started and ended at the Jämi airfield (61°46′43″N, 22°42′58″E, 154 m above sea level).

2.2 Airplane measurements

The University of Helsinki has organized several airborne measurement campaigns around Hyytiälä using an instrumented Cessna 172 airplane. Descriptions of the measurement setups can be found in previous studies (Leino et al., 2019; Schobesberger et al., 2013; Väänänen et al., 2016).

We used the particle number concentration in the 3-20 nm size range as an indication of particles that likely originated from NPF. The 3-20 nm particle number concentration was calculated by subtracting the total particle number concentration measured by the scanning mobility particle sizer (SMPS) in the size range 20-400 nm from the number concentration measured by the ultrafine condensation particle counter (UCPC). We skipped the smallest size bins of the SMPS because they were in some cases noisy.

In order to detect roll vortices on board the airplane we installed a turbulence probe (Aventech Research, AIMMS-20) at the end of the 2015 campaign. The AIMMS-20 was capable of measuring the the 3d wind vector at 20 Hz, but for the analysis we averaged the data to 1 s.

Typical measurement tracks consisted of ~30 km long flight segments flown roughly perpendicular to the mean wind direction over the same area while doing a single vertical profile from 100 m to 3000 m above ground (Figure 3). The ascend and descend speeds were ~1 m/s. The measurement airspeed was 36 m/s. Usually two 2.5 h flights were flown during a single day, one in the morning and one in the afternoon. Vertically the measurements covered all parts of the BL as well as the lowest kilometer of the free troposphere. The flights started and ended at the Tampere-Pirkkala airport (61°24′55″N, 23°35′16″E, 119 m above sea level).

2.3 Ground-based measurements

140 The airborne measurements were complemented by the measurements at the SMEAR II field station. The measurement station is located in Hyytiälä, Finland (61°50'40"N, 24°17'13"E, 180 m above sea level) and is surrounded by flat terrain and coniferous forest. The station represents the background conditions found in the boreal forest regions of northern latitudes (Hari and Kulmala, 2005).

145 The key aerosol instruments included in this study were the station's differential mobility particle sizer (DMPS) (Aalto et al., 2001), the NAIS (Manninen et al., 2009) and the particle size magnifier (PSM) (Vanhanen et al., 2011). The time resolutions of the DMPS and the NAIS were 10 min and 4 min respectively, from the NAIS we again used particle data from the positive polarity. The DMPS measured the particle number-size distribution in the size range 3-1000 nm. The PSM measured particle 150 number-size distribution between 1 and 2 nm and the time resolution was 12 min. The DMPS sampled the air from a vertical inlet at 8 m above the ground and the NAIS through a wall inlet at 2 m above the ground, both were inside the canopy. The PSM was sampling in a 35-m tall tower, above the forest canopy. The aerosol particle data from the station was not converted to standard conditions since the correction would be negligible.

155
Measurements of meteorological variables (temperature, relative humidity, wind direction and speed) and vertical particle flux from the station's mast (at 33.6 m above ground) were available at 1-min and 30-min time resolution respectively. The meteorological variables were measured at 33.6 m above ground. The system measuring the vertical particle flux used an ultrasonic 3d anemometer combined 160 with a condensation particle counter (CPC) at 23 m above ground. The CPC had a 10-nm cutoff size. The vertical particle flux was calculated using the eddy covariance method (Buzorius et al., 2000).

2.4 NPF event analysis

NPF event analysis, as described by Kulmala et al. (2012), was done for the flight measurement days. First the measurement days were classified by visual inspection into three different NPF event classes 165 (NPF event days, undefined days and nonevent days) based on the DMPS data. NPF event days display a continuously and smoothly growing particle mode starting from the smallest detectable size. This indicates a regional NPF event. On undefined days sub-25 nm particles are only intermittently (less than an hour) observed without apparent growth or a growing Aitken mode (25-100 nm) appears, possibly arising from a NPF episode elsewhere. On nonevent days no increase in sub-25 nm particle number 170 concentration is observed.

Particle growth rate (GR) is the rate of change of particle diameter. We used the so-called mode-fitting method to determine the particle GRs. The method involves fitting log-normal curves over the particle

size distributions on the growing particle mode, defining the peaks as the geometric mean particle diameters of the mode, and then using the change in the geometric mean diameter with respect to time to calculate the GR.

The formation rate of particles of the diameter d is defined as the rate at which the freshly-formed particles enter the size range $[d, d + \Delta d]$ as a result of their formation and growth. The formation rate J_d was calculated using the following equation (Kulmala et al., 2012):

$$\frac{dN_d}{dt} = J_d - \frac{GR}{\Delta d} \times N_d - CoagS_d \times N_d \qquad (2)$$

where N_d is the number concentration of particles in the size range $[d, d + \Delta d]$, GR is the growth rate and $CoagS_d$ is the coagulation sink for the particles in the size range. We calculated the $CoagS_d$ from the DMPS data and for the number concentrations we used NAIS data, so that the final time resolution of the formation rate was 4 min. The size ranges used from the NAIS data were 3-6 nm for J_3 and 10-20 nm for J_{10}.

2.5 Determination of BL height.

The height of the BL was determined from the aircraft measurements by inspecting the vertical profiles of relative humidity and potential temperature. The purpose was to determine if the roll-induced NPF events were observed inside the BL or above it.

We used two of the methods outlined by Seidel et al., (2010). The height of the BL was determined to be approximately at the altitude where there was a minimum vertical gradient in relative humidity and a maximum vertical gradient in potential temperature.

2.6 Detection of roll vortices

Inspecting satellite images for cloud streets was one way to deduce the presence of rolls (Etling and Brown, 1993). For this NASA's WorldView online tool was used. One limitation of this method was that clear sky rolls or rolls underneath a cloud cover could not be identified. Also the measurement flight time and the time of the satellite image were often separated by several hours and the meteorological conditions could change during that time.

The roll-axis can deviate from the mean BL flow direction (Miura, 1986) which causes the rolls to slowly move perpendicular to the mean BL flow direction, leaving low-frequency periodic variation in the time series of the wind components when measured from a stationary point (Buzorius et al., 2001;

Smedman, 1991). This provided us with one way to determine if roll circulation was taking place. The vertical and parallel to roll-axis wind components would always be in phase opposition while the phases of the perpendicular to roll-axis and parallel to roll-axis wind components would be separated by either 210   90 or -90 degrees depending on the direction of the roll movement (Brooks and Rogers, 1997; Vandemark et al., 2001). The variation in wind due to rolls could be directly observed in the smoothed wind components measured on board the airplane by the turbulence probe.

Insects tend to congregate at the updraft zones of rolls and they can be seen as clear air echoes by 215   weather radars (Wainwright et al., 2017; Wilson et al., 1994). In our case the Finnish Meteorological Institute's C-band (5.6 GHz) weather radar in Ikaalinen (61°46'1.6"N, 23°4'47.6"E, 154 m above sea level) provided information on the existence and location of planetary BL rolls. The analysis of the radar data was based on the processed radar imagery. Most of the flight-tracks were in the range 50 to 70 km from the radar, and during the summer season insects are usually abundant enough to let the rolls 220   be visible in the radar images over the area of airborne observations. The spatial resolution of the radar measurements is set by the antenna beam width and pulse duration. The Ikaalinen radar's resolution in the measurement range was 500 m, and the 1.0 degree beam gets about 1 km wide over the target area. Some small rolls may get unresolvable, because of the radar resolution, but more probably the detection would have been limited already by the weakness of the circulation of these tiny rolls to get enough 225   insects airborne high enough.

3 Results and discussion

Figure 4 shows a frequent observation in the ground-based aerosol particle measurements: a momentary increase in the number concentration of freshly formed clusters and aerosol particles during daytime, coupled with a relatively large fluctuation in the vertical particle flux. In Figure 4 the freshly formed 230   clusters and aerosol particles were observed between 10:00 and 12:00.

Concurrent airplane measurements flown over the measurement station on that day (Figure 5) showed that the location of increased aerosol particle number concentration was directly on top of the SMEAR II station. The increased number concentrations were observed over multiple overpasses indicating that 235   the concentrated zone was elongated along the mean wind direction. The vertical wind speed measurements on board the airplane revealed the presence of rolls as regularly alternating up- and downdrafts that were approximately aligned with the mean wind. The maximum number concentrations occurred in two adjacent roll downdrafts. Increased number concentrations were not observed above the BL, no pollution sources were close-by and the sky was cloudless.

240

Wind measurements from the mast of the measurement station (Figure 6) showed that roll vortices were slowly moving perpendicular to the mean wind (this is due to a slight difference in the directions of the mean wind and the roll axis, see Figure 7 for an illustration). The periodic anti-correlation between the horizontal and the vertical wind components is a clear indication of roll vortices drifting over the measurement location perpendicular to the mean wind direction. This explains why particles were observed only momentarily at the field station, they were connected to specific rolls that drifted over the station. Overall, the observations on this day show that the roll circulation was locally inducing the formation of new aerosol particles.

In Figure 6 one observes that the fluctuations in vertical particle flux do not match the fluctuations in vertical wind due to rolls. This is likely because of the following reason. During a sunny August day with moderate wind, turbulence dominates vertical transport close to the canopy, so the variations in particle number concentration and vertical particle flux close to the canopy are decoupled from the roll circulation. When the roll-induced NPF first moves over the field site the number concentration above the turbulent layer increases and the particles start to mix downwards. Inside the turbulent layer the particle flux becomes negative and the number concentration starts to increase. As more and more particles are mixed downwards, the number concentration increases inside the turbulent layer while the particle flux becomes less negative. As the roll-induced NPF moves away, the vertical particle flux can become positive if the number concentration below the flux measurement becomes higher than the number concentration above.

We defined two conditions to identify roll-induced NPF from the measurement data. Condition (i): a roughly 1-5 km wide region of increased sub-20 nm particle number concentration was observed on the flight track during consecutive overpasses when the airplane was flying perpendicular to the mean wind direction inside the BL. This implies a long and narrow region of freshly formed particles inside the BL that is roughly aligned with the mean wind (see Figure 8 for examples). Condition (ii): in the ground-based measurements the number concentration of sub-20 nm particles momentarily (lasting between 0.5-2 hours) increased, and this increase was associated with opposite fluctuations in the vertical particle flux (see Figure 9 for examples). This would be due to the roll-induced NPF moving over the measurement station and it requires that the rolls are not aligned with the mean BL flow.

The roll-induced NPF condition (ii) never occurred at the same time without condition (i) being also true, but condition (i) did occur without condition (ii). This is likely because when the rolls were not aligned with the mean wind the roll-induced NPF could be observed from the airplane as well as from the station, whereas if the rolls were aligned with the mean wind, then the roll-induced NPF could still be observed from the airplane but not from the measurement station.

The airborne measurement data was classified with respect to NPF events and for the presence of roll vortices and roll-induced NPF. Roll-induced NPF was observed on 30% (6/20) of the regional NPF event days and on 22% (8/36) of the days classified as undefined (Figure 10A). According to radar and satellite observations the counter-rotating horizontal circulations were always present during the roll-induced NPF (Figure 10B) and according to Fisher's exact test this association was statistically significant (p=0.03). Roll vortices do not guarantee that roll-induced NPF occurs, since many other factors, such as a sufficient amount of sunlight and low enough sinks for low-volatile vapors and small clusters, are also important in determining whether atmospheric NPF may occur or not (Dada et al., 2017; Hamed et al., 2007).

The timescale that a roll-induced NPF moves over the measurement station is roughly an hour. This timescale is similar to the period of a typical roll vortex and it allows us to estimate the total effect of a roll on NPF. Using condition (ii), we identified some of the clearest cases of roll-induced NPF (29 days and 46 roll-induced NPF events) from only the ground-based measurements during 2006-2017.

Multiple roll-induced NPF events during a single day were observed on 13/29 days. In these cases by looking at the change in particle diameter between subsequent roll-induced NPF events we were able to estimate the GR. In addition, on May 8, 2013 we could calculate the *GR* from a single roll-induced NPF event by following it with the zeppelin aircraft (Figure 11). We found that the median GR of the roll-induced NPF particles was 1.9 (inter quartile range (IQR) = 1.3-2.1) nm/h. The median size range for the GR estimation was 7.5-15 nm. This is similar to the median GR of 2.5 nm/h for 3-25 nm particles reported by Nieminen et al., (2014) for regional-scale NPF events observed at the station.

We aggregated all the roll-induced NPF observations into 1-hour-averaged bins using the median GR and the geometric mean diameters of the particles, assuming that the particles were formed at *t=0* hours (Figure 12).

Then we calculated the formation rates and their uncertainties. We assumed that the roll-induced NPF GRs were normally distributed with mean equal to the median GR and standard deviation given by the magnitude of the IQR. We randomly sampled a GR from the distribution and distributed the roll-induced NPF observations into 1-hour bins. For each 1-hour bin we assumed that the number-size distributions again followed a normal distribution with mean equal to the median and standard deviation given by the IQR. We randomly sampled a number-size distribution from each bin and calculated the formation rates based on that. We repeated this procedure 1000 times in order to estimate the J_3 and J_{10} and their uncertainties shown in Figure 12.

The resulting peak formation rate was 2.4 (IQR=1.6-3.1) $cm^{-3}s^{-1}$ for 3-nm particles and 0.4 (IQR = 0.2-0.6) $cm^{-3}s^{-1}$ for 10-nm particles. Nieminen et al., (2014) found that for regional-scale NPF events during springtime, the median formation rates of 3-nm and 10-nm particles were 1.0 $cm^{-3} s^{-1}$ and 0.52 $cm^{-3} s^{-1}$, respectively.

In addition, we estimated the fraction of area covered by the roll-induced NPF. We assumed that the roll-induced NPF events extend much longer along the rolls, which is supported by the aircraft data. This means that for the area fraction we need to estimate what the spacing of the roll-induced NPF events is perpendicular to the direction of the rolls.

If the wind conditions stay the same during the period when the multiple roll-induced NPF events move over the station, then we can assume that the rolls move over the station at a steady pace. This means that dividing the time that subsequent roll-induced NPF events observed during the same day spent on top of the measurement station by the total time it took for the roll-induced NPF events to move over the site can be used as an area fraction estimate. According to measurements from the mast, on average the wind conditions during the observations did not change significantly.

We found that the fraction of area covered by the roll-induced NPF was 0.46 (IQR = 0.39-0.64). The roll systems are regionally roughly homogeneous (as demonstrated by cloud streets caused by the rolls in satellite images), so we can assume that the fraction of area covered by the roll-induced NPF events applies regionally and the phenomena is not limited to the close vicinity of the site.

We combined the median formation rates, the median area coverage and the statistics obtained from the aircraft campaigns and estimated using Equation 3 how much, in terms of percentage increase, the roll-induced NPF enhances the production of new aerosol particles in Hyytiälä.

$$J_d \text{ enhancement} = \frac{A(\text{roll-induced}) \times n(\text{roll-induced}) \times J_d(\text{roll-induced})}{n(\text{regional}) \times J_d(\text{regional})} \times 100\%. \qquad (3)$$

Here, A is the median area fraction, n is the number of roll-induced and regional NPF events observed and J_d is the median formation rate of particles at the diameter d. The uncertainty was calculated by using the propagation of uncertainty. We estimate that compared with only regional NPF, the roll-induced NPF enhances the production of new aerosol particles by 83±34% and 26±8% for 3-nm and 10-nm particles respectively. In addition to the enhancement of regional NPF, there were several days

during which practically no NPF would have taken place without roll-induced NPF, such as the case study in Figure 4.

4 Conclusions

350 We studied what is the effect of roll vortices on atmospheric NPF in the BL by analyzing airborne and ground-based measurements done over a rural boreal forest in southern Finland. We found that roll-induced NPF can considerably enhance the production of new aerosol particles over a boreal forest and these particles can grow to larger, potentially CCN, sizes, similar to particles produced by regional NPF. Roll-induced NPF seems to occur in only some of the roll vortices, which is likely related to variability

355 in the rolls. In order to fully understand roll-induced NPF, better measurement and analysis methods need to be developed. For example measuring the fluxes of sub-10 nm particles and doing airborne flux measurements. More measurements with the turbulence probe on board need to be performed. It would also be interesting to study the cluster composition during roll-induced NPF.

360 NPF is a ubiquitous phenomenon in the global atmosphere (Kerminen et al., 2018; Kulmala et al., 2004), likewise roll vortices are a common feature in the planetary BL around the world (Atkinson and Wu Zhang, 1996; Etling and Brown, 1993; Young et al., 2002). Therefore, roll-induced NPF is expected to take place in several other environments around the world as well. Hence, unstable stratification and the formation of roll vortices needs to be taken into account in order to understand the overall role of

365 atmospheric NPF in particle number and CCN budgets.

Author contribution: JL, KL, RV, AM, SBM, HEM and JK carried out the airborne measurements. ML processed and interpreted the weather radar data. MB, SZ and HJ helped with the analysis of

370 meteorological data. JL prepared the manuscript with contributions from all co-authors.

Acknowledgements: This project has received funding from the ERC advanced grant No. 742206, the European Union's Horizon 2020 research and innovation program under grant agreement No. 654109, the Academy of Finland Center of Excellence project No. 272041 and the European Commission under

375 the Framework Programme 7 (FP7-ENV-2010-265148). S. Zilitinkevich acknowledges support from the Academy of Finland projects ABBA No. 280700 (2014-2017) and ClimEco No. 314 798/799 (2018-2020); and Russian Science Foundation project No. 15-17-20009 (2015-2018). We appreciate the efforts that the Zeppelin NT pilots and ground crews made to this work. We acknowledge Dr. T. F. Mentel and Dr. F. Rohrer from Forschungszentrum Jülich, Germany. We thank Erkki Järvinen and the pilots at

380 Airspark Oy for operating the research airplane. We acknowledge the use of imagery from the NASA

Worldview application (https://worldview.earthdata.nasa.gov/) operated by the NASA/Goddard Space Flight Center Earth Science Data and Information System (ESDIS) project.

References

Aalto, P., Hämeri, K., Becker, E., Weber, R., Salm, J., Mäkelä, J. M., Hoell, C., O'Dowd, C. D., Hansson, H.-C., Väkevä, M., Koponen, I. K., Buzorius, G. and Kulmala, M.: Physical characterization of aerosol particles during nucleation events, Tellus B, 53(4), 344–358, doi:10.3402/tellusb.v53i4.17127, 2001.

Atkinson, B. W. and Wu Zhang, J.: Mesoscale shallow convection in the atmosphere, Rev. Geophys., 34(4), 403–431, doi:10.1029/96RG02623, 1996.

Boucher, O., Randall, D., Artaxo, P., Bretherton, C., Feingold, G., Forster, P., Kerminen, V.-M., Kondo, Y., Liao, H., Lohmann, U., Rasch, P., Satheesh, S. K., Sherwood, S., Stevens, B. and Zhang, X. Y.: Clouds and Aerosols, in Climate Change 2013: The Physical Science Basis. Contribution of Working Group I to the Fifth Assessment Report of the Intergovernmental Panel on Climate Change, edited by T. F. Stocker, D. Qin, G.-K. Plattner, M. Tignor, S. K. Allen, J. Boschung, A. Nauels, Y. Xia, V. Bex, and P. M. Midgley, pp. 571–658, Cambridge University Press, Cambridge, United Kingdom and New York, NY, USA. [online] Available from: www.climatechange2013.org, 2013.

Brooks, I. M. and Rogers, D. P.: Aircraft Observations of Boundary Layer Rolls off the Coast of California, J. Atmospheric Sci., 54(14), 1834–1849, doi:10.1175/1520-0469(1997)054<1834:AOOBLR>2.0.CO;2, 1997.

Buzorius, G., Rannik, Ü., Mäkelä, J. M., Keronen, P., Vesala, T. and Kulmala, M.: Vertical aerosol fluxes measured by the eddy covariance method and deposition of nucleation mode particles above a Scots pine forest in southern Finland, J. Geophys. Res. Atmospheres, 105(D15), 19905–19916, doi:10.1029/2000JD900108, 2000.

Buzorius, G., Rannik, Ü., Nilsson, D. and Kulmala, M.: Vertical fluxes and micrometeorology during aerosol particle formation events, Tellus B, 53(4), 394–405, doi:10.1034/j.1600-0889.2001.530406.x, 2001.

Crumeyrolle, S., Manninen, H. E., Sellegri, K., Roberts, G., Gomes, L., Kulmala, M., Weigel, R., Laj, P. and Schwarzenboeck, A.: New particle formation events measured on board the ATR-42 aircraft during the EUCAARI campaign, Atmospheric Chem. Phys., 10(14), 6721–6735, doi:10.5194/acp-10-6721-2010, 2010.

Dada, L., Paasonen, P., Nieminen, T., Buenrostro Mazon, S., Kontkanen, J., Peräkylä, O., Lehtipalo, K., Hussein, T., Petäjä, T., Kerminen, V.-M., Bäck, J. and Kulmala, M.: Long-term analysis of clear-sky new particle formation events and nonevents in Hyytiälä, Atmos Chem Phys, 17(10), 6227–6241, doi:10.5194/acp-17-6227-2017, 2017.

Dunne, E. M., Gordon, H., Kürten, A., Almeida, J., Duplissy, J., Williamson, C., Ortega, I. K., Pringle, K. J., Adamov, A., Baltensperger, U., Barmet, P., Benduhn, F., Bianchi, F., Breitenlechner, M., Clarke, A., Curtius, J., Dommen, J., Donahue, N. M., Ehrhart, S., Flagan, R. C., Franchin, A., Guida, R., Hakala, J., Hansel, A., Heinritzi, M., Jokinen, T., Kangasluoma, J., Kirkby, J., Kulmala, M., Kupc, A., Lawler, M. J., Lehtipalo, K., Makhmutov, V., Mann, G., Mathot, S., Merikanto, J., Miettinen, P., Nenes, A., Onnela, A., Rap, A., Reddington, C. L. S., Riccobono, F., Richards, N. A. D., Rissanen, M. P., Rondo, L., Sarnela, N., Schobesberger, S., Sengupta, K., Simon, M., Sipilä, M., Smith, J. N., Stozkhov, Y., Tomé, A., Tröstl, J., Wagner, P. E., Wimmer, D., Winkler, P. M., Worsnop, D. R. and Carslaw, K. S.: Global atmospheric particle formation from CERN CLOUD measurements, Science, 354(6316), 1119–1124, doi:10.1126/science.aaf2649, 2016.

Easter, R. C. and Peters, L. K.: Binary homogeneous nucleation: temperature and relative humidity fluctuations, nonlinearity, and aspects of new particle production in the atmosphere, J. Appl. Meteorol., 33(7), 775–784, doi:10.1175/1520-0450(1994)033<0775:BHNTAR>2.0.CO;2, 1994.

Ehn, M., Thornton, J. A., Kleist, E., Sipilä, M., Junninen, H., Pullinen, I., Springer, M., Rubach, F., Tillmann, R., Lee, B., Lopez-Hilfiker, F., Andres, S., Acir, I.-H., Rissanen, M., Jokinen, T., Schobesberger, S., Kangasluoma, J., Kontkanen, J., Nieminen, T., Kurtén, T., Nielsen, L. B., Jørgensen, S., Kjaergaard, H. G., Canagaratna, M., Maso, M. D., Berndt, T., Petäjä, T., Wahner, A., Kerminen, V.-M., Kulmala, M., Worsnop, D. R., Wildt, J. and Mentel, T. F.: A large source of low-volatility secondary organic aerosol, Nature, 506(7489), 476–479, doi:10.1038/nature13032, 2014.

Etling, D. and Brown, R. A.: Roll vortices in the planetary boundary layer: A review, Bound.-Layer Meteorol., 65(3), 215–248, doi:10.1007/BF00705527, 1993.

Gordon, H., Kirkby, J., Baltensperger, U., Bianchi, F., Breitenlechner, M., Curtius, J., Dias, A., Dommen, J., Donahue, N. M., Dunne, E. M., Duplissy, J., Ehrhart, S., Flagan, R. C., Frege, C., Fuchs, C., Hansel, A., Hoyle, C. R., Kulmala, M., Kürten, A., Lehtipalo, K., Makhmutov, V., Molteni, U., Rissanen, M. P., Stozkhov, Y., Tröstl, J., Tsagkogeorgas, G., Wagner, R., Williamson, C., Wimmer, D., Winkler, P. M., Yan, C. and Carslaw, K. S.: Causes and importance of new particle formation in

the present-day and preindustrial atmospheres, J. Geophys. Res. Atmospheres, 122(16), 8739–8760, doi:10.1002/2017JD026844, 2017.

Gormley, P. G. and Kennedy, M.: Diffusion from a Stream Flowing through a Cylindrical Tube, Proc. R. Ir. Acad. Sect. Math. Phys. Sci., 52, 163–169, 1948.

Gryspeerdt, E., Stier, P. and Partridge, D. G.: Satellite observations of cloud regime development: the role of aerosol processes, Atmospheric Chem. Phys., 14(3), 1141–1158, doi:https://doi.org/10.5194/acp-14-1141-2014, 2014.

Hamed, A., Joutsensaari, J., Mikkonen, S., Sogacheva, L., Dal Maso, M., Kulmala, M., Cavalli, F., Fuzzi, S., Facchini, M. C., Decesari, S., Mircea, M., Lehtinen, K. E. J. and Laaksonen, A.: Nucleation and growth of new particles in Po Valley, Italy, Atmos Chem Phys, 7(2), 355–376, doi:10.5194/acp-7-355-2007, 2007.

Hari, P. and Kulmala, M.: Station for measuring ecosystem-atmosphere relations (SMEAR II), Boreal Environ. Res., 10(5), 315–322, 2005.

Kerminen, V.-M., Paramonov, M., Anttila, T., Riipinen, I., Fountoukis, C., Korhonen, H., Asmi, E., Laakso, L., Lihavainen, H., Swietlicki, E., Svenningsson, B., Asmi, A., Pandis, S. N., Kulmala, M. and Petäjä, T.: Cloud condensation nuclei production associated with atmospheric nucleation: a synthesis based on existing literature and new results, Atmospheric Chem. Phys., 12(24), 12037–12059, doi:https://doi.org/10.5194/acp-12-12037-2012, 2012.

Kerminen, V.-M., Chen, X., Vakkari, V., Petäjä, T., Kulmala, M. and Bianchi, F.: Atmospheric new particle formation and growth: review of field observations, Environ. Res. Lett., 13(10), 103003, doi:10.1088/1748-9326/aadf3c, 2018.

Kulmala, M., Vehkamäki, H., Petäjä, T., Dal Maso, M., Lauri, A., Kerminen, V.-M., Birmili, W. and McMurry, P. H.: Formation and growth rates of ultrafine atmospheric particles: a review of observations, J. Aerosol Sci., 35(2), 143–176, doi:10.1016/j.jaerosci.2003.10.003, 2004.

Kulmala, M., Petäjä, T., Nieminen, T., Sipilä, M., Manninen, H. E., Lehtipalo, K., Dal Maso, M., Aalto, P. P., Junninen, H., Paasonen, P., Riipinen, I., Lehtinen, K. E. J., Laaksonen, A. and Kerminen, V.-M.: Measurement of the nucleation of atmospheric aerosol particles, Nat. Protoc., 7(9), 1651–1667, doi:10.1038/nprot.2012.091, 2012.

Leino, K., Lampilahti, J., Poutanen, P., Väänänen, R., Manninen, A., Buenrostro Mazon, S., Dada, L., Franck, A., Wimmer, D., Aalto, P. P., Ahonen, L. R., Enroth, J., Kangasluoma, J., Keronen, P., Korhonen, F., Laakso, H., Matilainen, T., Siivola, E., Manninen, H. E., Lehtipalo, K., Kerminen, V.-M., Petäjä, T. and Kulmala, M.: Vertical profiles of sub-3 nm particles over the boreal forest, Atmospheric Chem. Phys., 19(6), 4127–4138, doi:https://doi.org/10.5194/acp-19-4127-2019, 2019.

Manninen, H. E., Petäjä, T., Asmi, E., Riipinen, N., Nieminen, T., Mikkilä, J., Horrak, U., Mirme, A., Mirme, S., Laakso, L., Kerminen, V.-M. and Kulmala, M.: Long-term field measurements of charged and neutral clusters using Neutral cluster and Air Ion Spectrometer (NAIS), Boreal Environ. Res., 14(4), 591–605, 2009.

Mirme, S. and Mirme, A.: The mathematical principles and design of the NAIS – a spectrometer for the measurement of cluster ion and nanometer aerosol size distributions, Atmospheric Meas. Tech., 6(4), 1061–1071, doi:10.5194/amt-6-1061-2013, 2013.

Mirme, S., Mirme, A., Minikin, A., Petzold, A., Hõrrak, U., Kerminen, V.-M. and Kulmala, M.: Atmospheric sub-3 nm particles at high altitudes, Atmospheric Chem. Phys., 10(2), 437–451, doi:10.5194/acp-10-437-2010, 2010.

Miura, Y.: Aspect ratios of longitudinal rolls and convection cells observed during cold air outbreaks, J. Atmospheric Sci., 43(1), 26–39, doi:10.1175/1520-0469(1986)043<0026:AROLRA>2.0.CO;2, 1986.

Nieminen, T., Asmi, A., Dal Maso, M., Aalto, P. P., Keronen, P., Petäjä, T., Kulmala, M. and Kerminen, V.-M.: Trends in atmospheric new-particle formation: 16 years of observations in a boreal-forest environment, Boreal Environ. Res., 19, 191–214, 2014.

Nilsson, E. D. and Kulmala, M.: The potential for atmospheric mixing processes to enhance the binary nucleation rate, J. Geophys. Res. Atmospheres, 103(D1), 1381–1389, doi:10.1029/97JD02629, 1998.

Nilsson, E. D., Rannik, Ü., Kulmala, M., Buzorius, G. and O'dowd, C. D.: Effects of continental boundary layer evolution, convection, turbulence and entrainment, on aerosol formation, Tellus B, 53(4), 441–461, doi:10.1034/j.1600-0889.2001.530409.x, 2001.

O'Dowd, C. D., Yoon, Y. J., Junkermann, W., Aalto, P., Kulmala, M., Lihavainen, H. and Viisanen, Y.: Airborne measurements of nucleation mode particles II: boreal forest nucleation events, Atmospheric Chem. Phys., 9(3), 937–944, doi:10.5194/acp-9-937-2009, 2009.

Platis, A., Altstädter, B., Wehner, B., Wildmann, N., Lampert, A., Hermann, M., Birmili, W. and Bange, J.: An Observational Case Study on the Influence of Atmospheric Boundary-Layer Dynamics on New Particle Formation, Bound.-Layer Meteorol., 158(1), 67–92, doi:10.1007/s10546-015-0084-y, 2015.

Rosenfeld, D., Andreae, M. O., Asmi, A., Chin, M., Leeuw, G. de, Donovan, D. P., Kahn, R., Kinne, S., Kivekäs, N., Kulmala, M., Lau, W., Schmidt, K. S., Suni, T., Wagner, T., Wild, M. and Quaas, J.: Global observations of aerosol-cloud-precipitation-climate interactions, Rev. Geophys., 52(4), 750–808, doi:10.1002/2013RG000441, 2014.

Schobesberger, S., Väänänen, R., Leino, K., Virkkula, A., Backman, J., Pohja, T., Siivola, E., Franchin, A., Mikkilä, J., Paramonov, M., Aalto, P. P., Krejci, R., Petäjä, T. and Kulmala, M.: Airborne measurements over the boreal forest of southern Finland during new particle formation events in 2009 and 2010, Boreal Environ. Res., 18(2), 145–164, 2013.

Seidel, D. J., Ao, C. O. and Li, K.: Estimating climatological planetary boundary layer heights from radiosonde observations: Comparison of methods and uncertainty analysis, J. Geophys. Res. Atmospheres, 115(D16), D16113, doi:10.1029/2009JD013680, 2010.

Siebert, H., Stratmann, F. and Wehner, B.: First observations of increased ultrafine particle number concentrations near the inversion of a continental planetary boundary layer and its relation to ground-based measurements, Geophys. Res. Lett., 31(9), doi:10.1029/2003GL019086, 2004.

Smedman, A.-S.: Occurrence of roll circulations in a shallow boundary layer, Bound.-Layer Meteorol., 57(4), 343–358, doi:10.1007/BF00120053, 1991.

Väänänen, R., Krejci, R., Manninen, H. E., Manninen, A., Lampilahti, J., Buenrostro Mazon, S., Nieminen, T., Yli-Juuti, T., Kontkanen, J., Asmi, A., Aalto, P. P., Keronen, P., Pohja, T., O'Connor, E., Kerminen, V.-M., Petäjä, T. and Kulmala, M.: Vertical and horizontal variation of aerosol number size distribution in the boreal environment, Atmospheric Chem. Phys. Discuss., Manuscript in review, doi:10.5194/acp-2016-556, 2016.

Vandemark, D., Mourad, P. D., Bailey, S. A., Crawford, T. L., Vogel, C. A., Sun, J. and Chapron, B.: Measured changes in ocean surface roughness due to atmospheric boundary layer rolls, J. Geophys. Res. Oceans, 106(C3), 4639–4654, doi:10.1029/1999JC000051, 2001.

Vanhanen, J., Mikkilä, J., Lehtipalo, K., Sipilä, M., Manninen, H. E., Siivola, E., Petäjä, T. and Kulmala, M.: Particle size magnifier for nano-CN detection, Aerosol Sci. Technol., 45(4), 533–542, doi:10.1080/02786826.2010.547889, 2011.

Wainwright, C. E., Stepanian, P. M., Reynolds, D. R. and Reynolds, A. M.: The movement of small insects in the convective boundary layer: linking patterns to processes, Sci. Rep., 7(1), 5438, doi:10.1038/s41598-017-04503-0, 2017.

Wehner, B., Siebert, H., Ansmann, A., Ditas, F., Seifert, P., Stratmann, F., Wiedensohler, A., Apituley, A., Shaw, R. A., Manninen, H. E. and Kulmala, M.: Observations of turbulence-induced new particle formation in the residual layer, Atmospheric Chem. Phys., 10(9), 4319–4330, doi:10.5194/acp-10-4319-2010, 2010.

Wilson, J. W., Weckwerth, T. M., Vivekanandan, J., Wakimoto, R. M. and Russell, R. W.: Boundary layer clear-air radar echoes: Origin of echoes and accuracy of derived winds, J. Atmospheric Ocean. Technol., 11(5), 1184–1206, doi:10.1175/1520-0426(1994)011<1184:BLCARE>2.0.CO;2, 1994.

Young, G. S., Kristovich, D. A., Hjelmfelt, M. R. and Foster, R. C.: Rolls, streets, waves and more: A review of quasi-two-dimensional structures in the atmospheric boundary layer, Bull. Am. Meteorol. Soc., 83(7), ES54–ES69, 2002.

Zilitinkevich, S. S., Hunt, J. C. R., Esau, I. N., Grachev, A. A., Lalas, D. P., Akylas, E., Tombrou, M., Fairall, C. W., Fernando, H. J. S., Baklanov, A. A. and Joffre, S. M.: The influence of large convective eddies on the surface-layer turbulence, Q. J. R. Meteorol. Soc., 132(618), 1426–1456, doi:10.1256/qj.05.79, 2006.
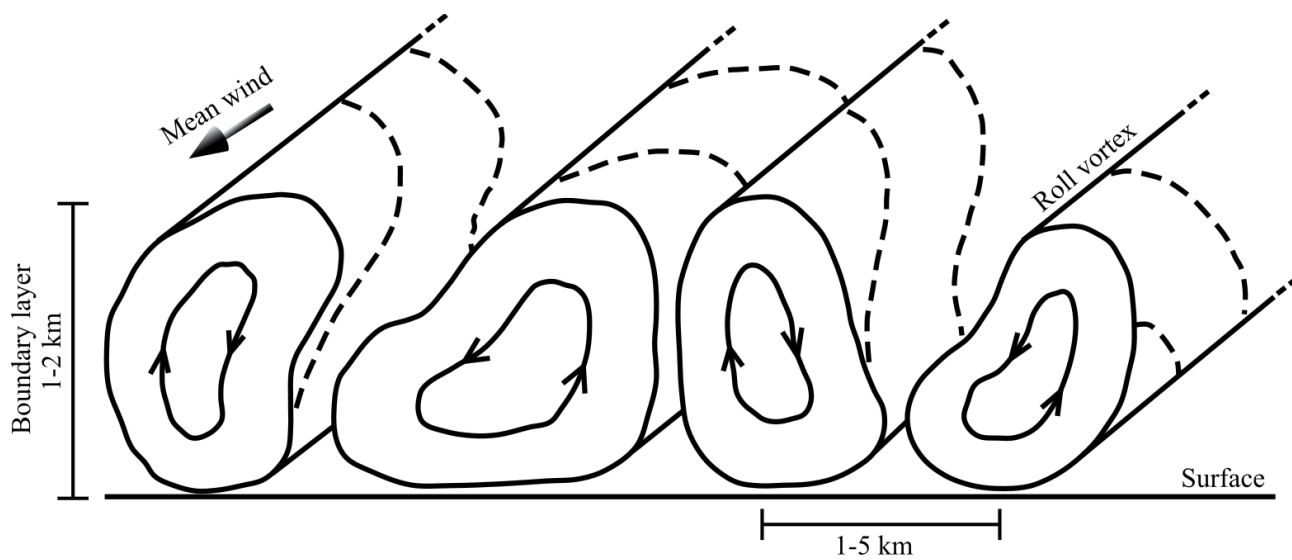
385
Figure 1: A schematic drawing of roll vortices in the boundary layer.
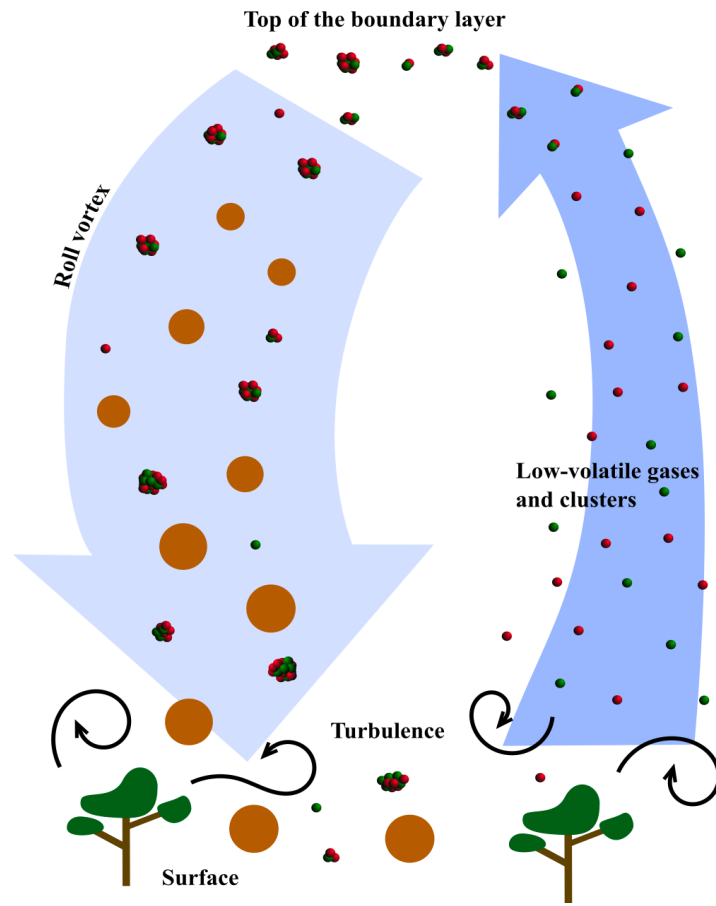
Figure 2: A schematic illustration of roll-induced NPF when viewed along a roll.
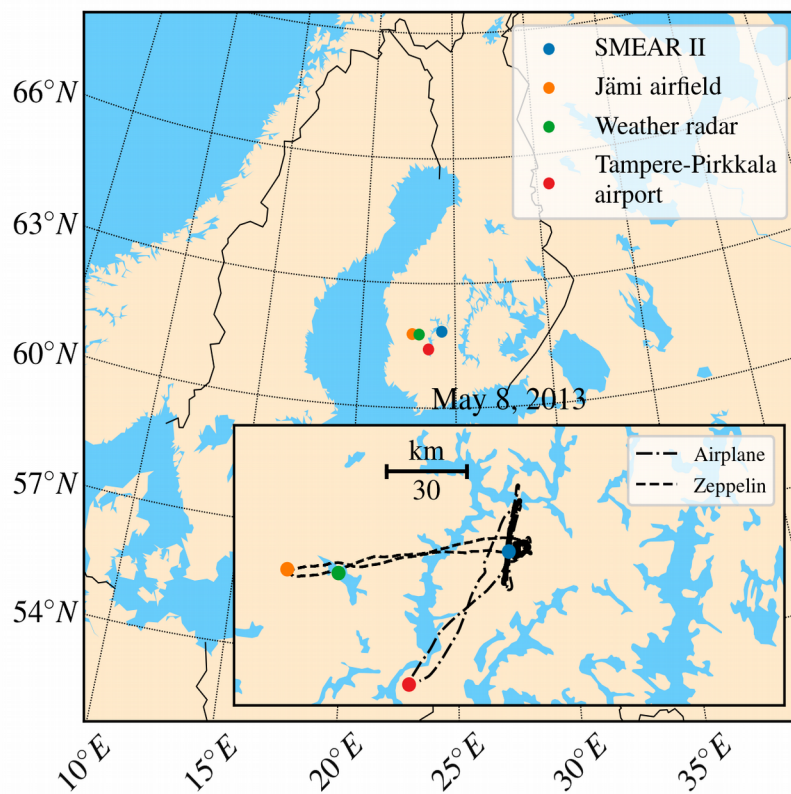
Figure 3: The locations of the Tampere-Pirkkala airport (ICAO: EFTP), Jämi airfield (ICAO: EFJM), Ikaalinen weather radar and SMEAR II station marked on a map. As an example, the aircraft measurement tracks on May 8, 2013 are included.
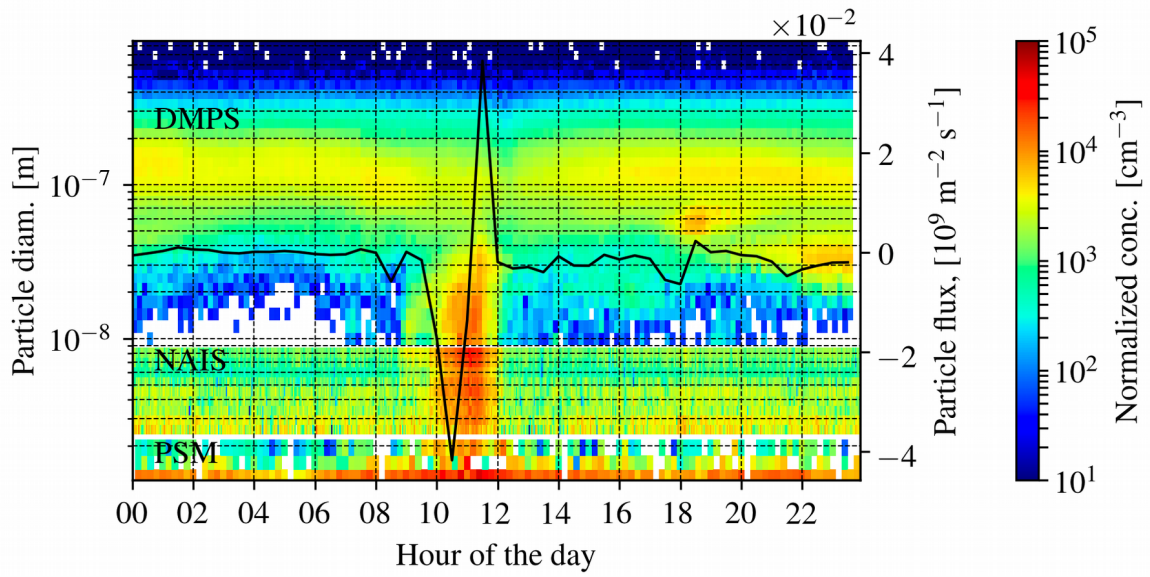
Figure 4: The particle number-size distribution in the range 1-1000 nm (composite of PSM, NAIS and DMPS data, see the Methods for instrument details) measured at the SMEAR II station on August 21, 2015. The black line is the vertical flux of >10 nm particles measured above the forest canopy (23 m height, negative sign means downward flux).
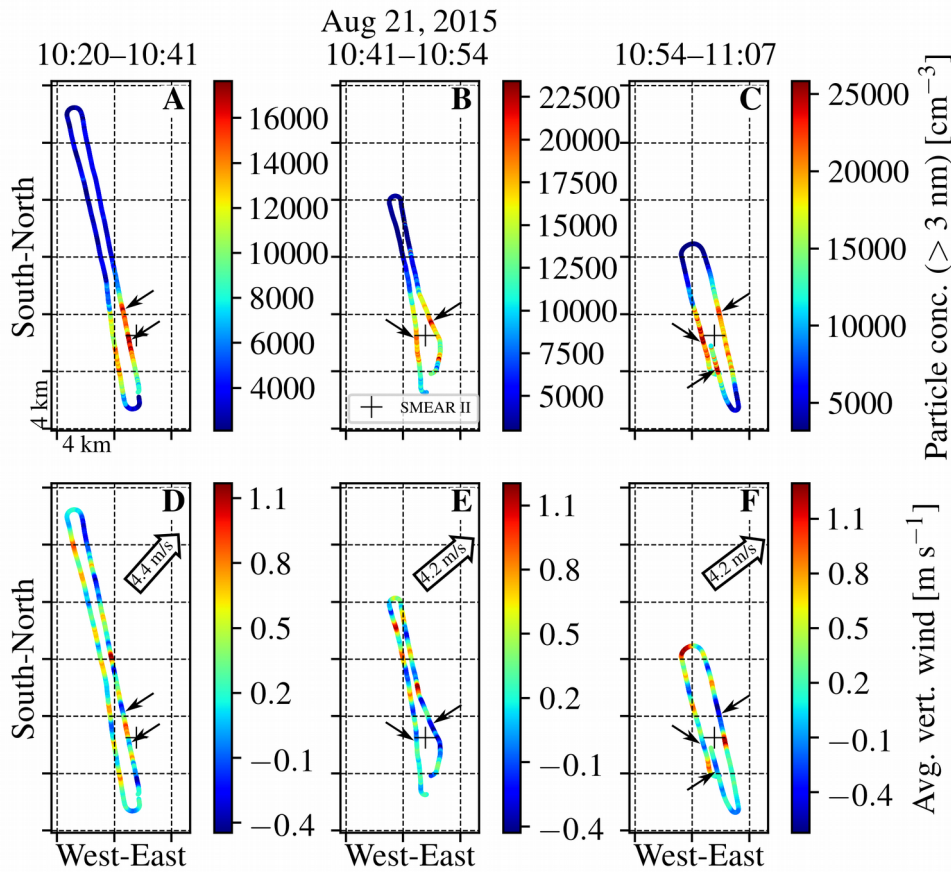
Figure 5: In panels A-C the sections of the measurement aiplane's flight track are colored by >3 nm particle number concentration. The grids have a 4-by-4 km spacing, the plus sign marks the position of the SMEAR II station and the time intervals for the flight track sections are displayed on top of the panels. In panels D-F the same flight tracks are colored by vertical wind speed smoothed using 30-sec moving average. The positive sign refers to updraft and the negative sign to downdraft. The large arrows show the mean wind speed and direction measured on board the airplane. The flight tracks were flown inside the convective BL between 120 m and 620 m above ground. The small arrows show that the maxima in the particle number concentration were located in the roll downdrafts.
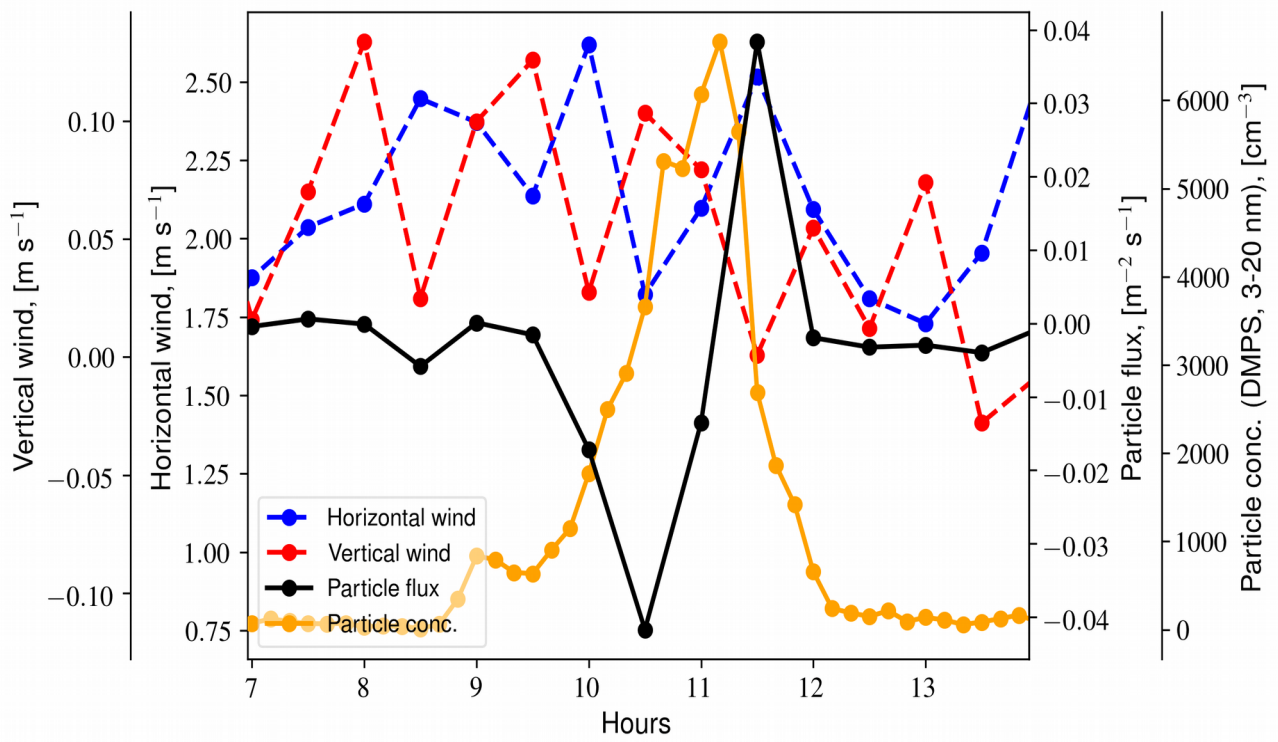
Figure 6: Time series of the vertical wind (33.6 m above ground), horizontal wind (33.6 m above ground), vertical flux of >10 nm particles (23 m above ground) and number concentration of 3-20 nm particles inside the canopy (8 m above ground) on Aug 21, 2015.

405
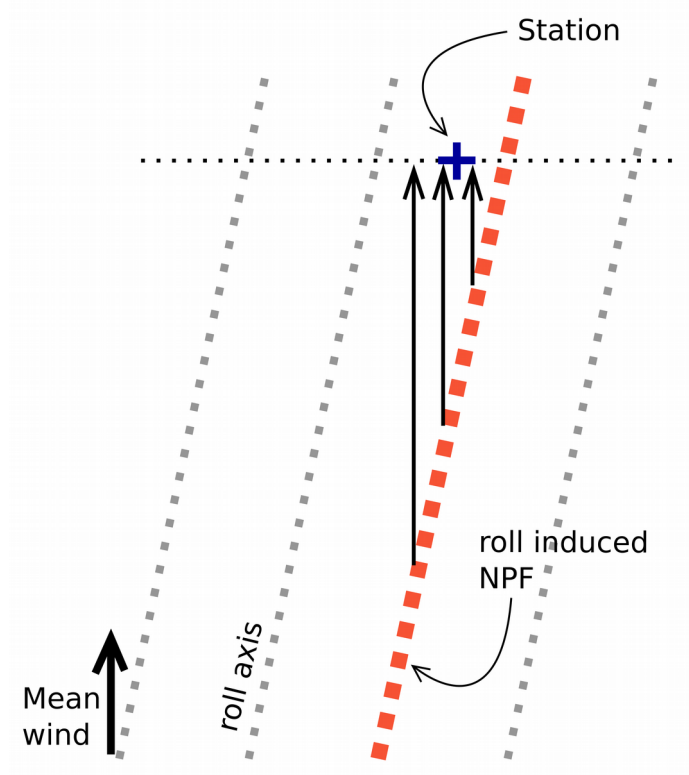
410 **Figure 7:** Schematic diagram illustrating how a difference in the direction of the mean wind and the roll axis causes the rolls (and the roll-induced NPF) to move over a stationary point perpendicular to the mean wind direction.
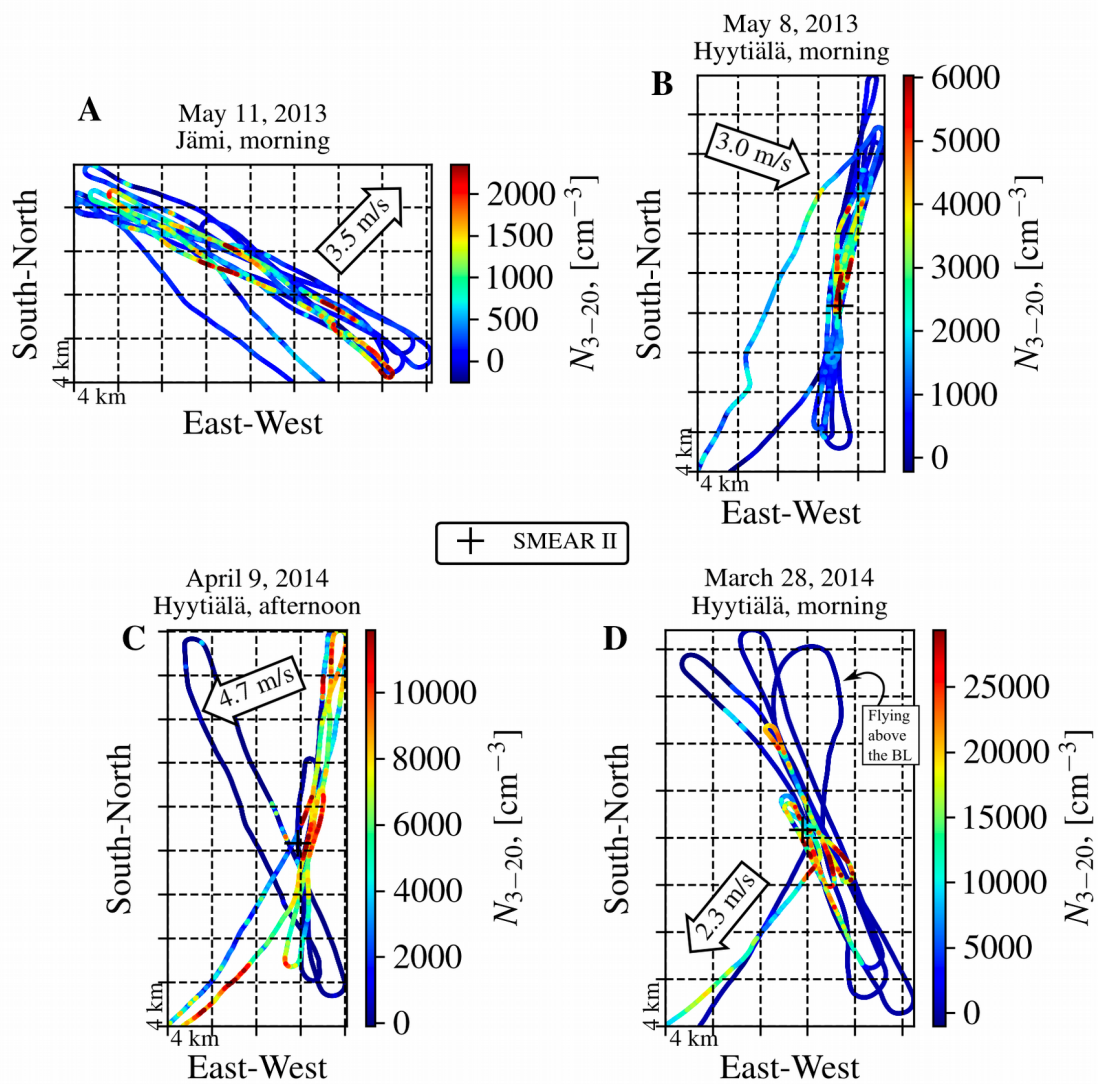
Figure 8: Panels A-D show the research airplane's flight tracks colored by particle number concentration in the 3-20 nm diameter range on four different measurement flights. The higher particle number concentrations are displayed on top in order to make the roll-induced NPF more clearly visible. The arrows show the mean wind direction and speed from the SMEAR II mast.
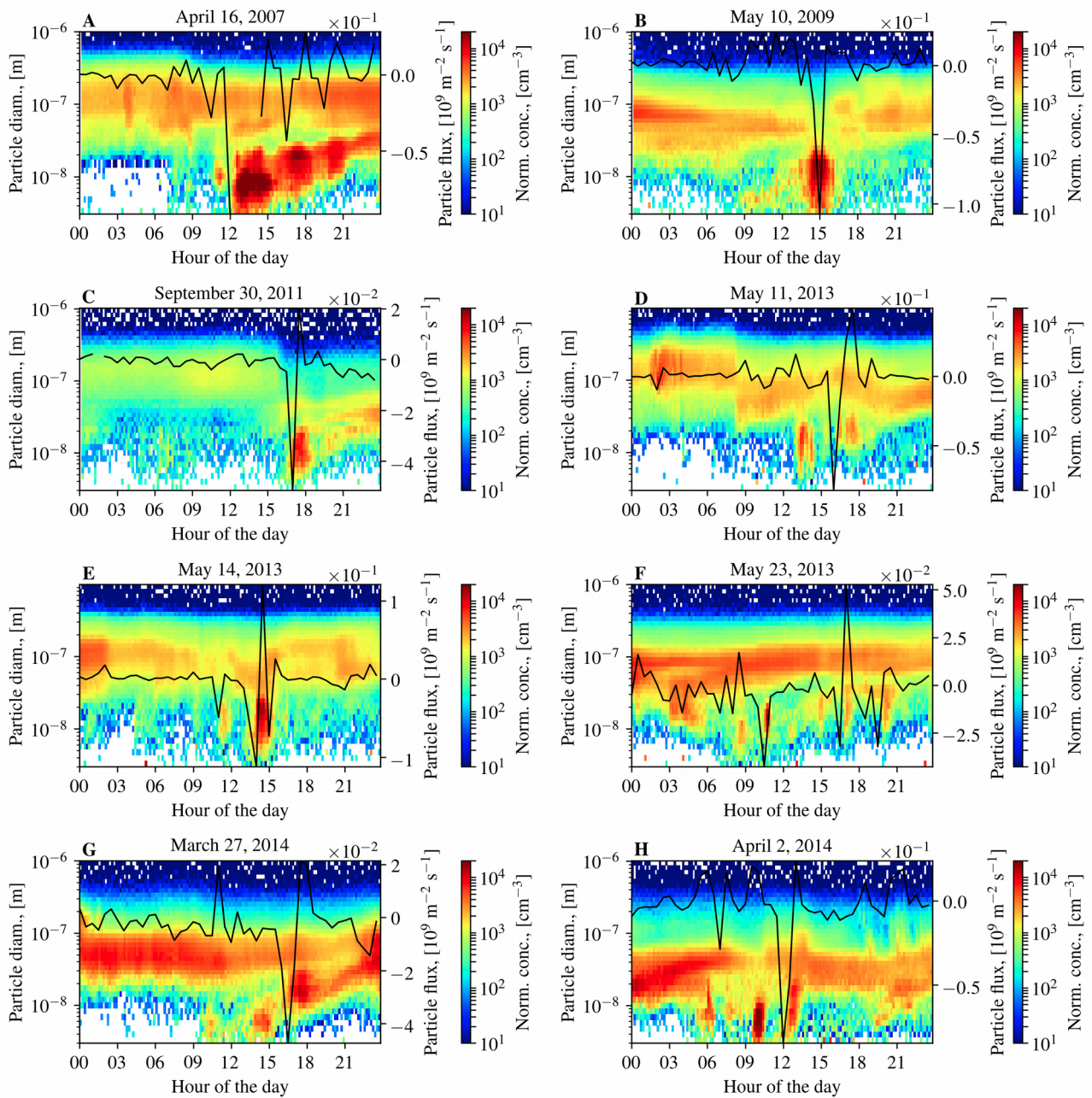
Figure 9: The panels A-H show 3-1000 nm particle number-size distribution measured at the SMEAR II station by the DMPS during some of the days when there was roll-induced NPF. In addition the black line shows the vertical flux of >10 nm particles measured at 23 m height.
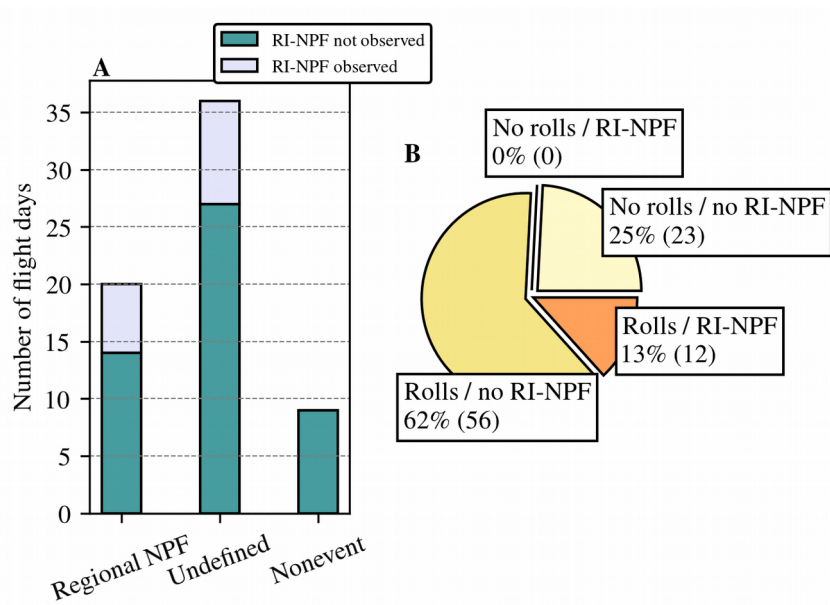
Figure 10: Panel A shows how the roll-induced NPF (RI-NPF) observations distribute into different NPF event classes on the flight days. Panel B shows the classification of each measurement flight into four different classes based on whether rolls and/or RI-NPF over the same area was observed or not. Note that the data in panel A consists of flight days while the data in panel B consists of individual flights (there could be more than one flight per day).
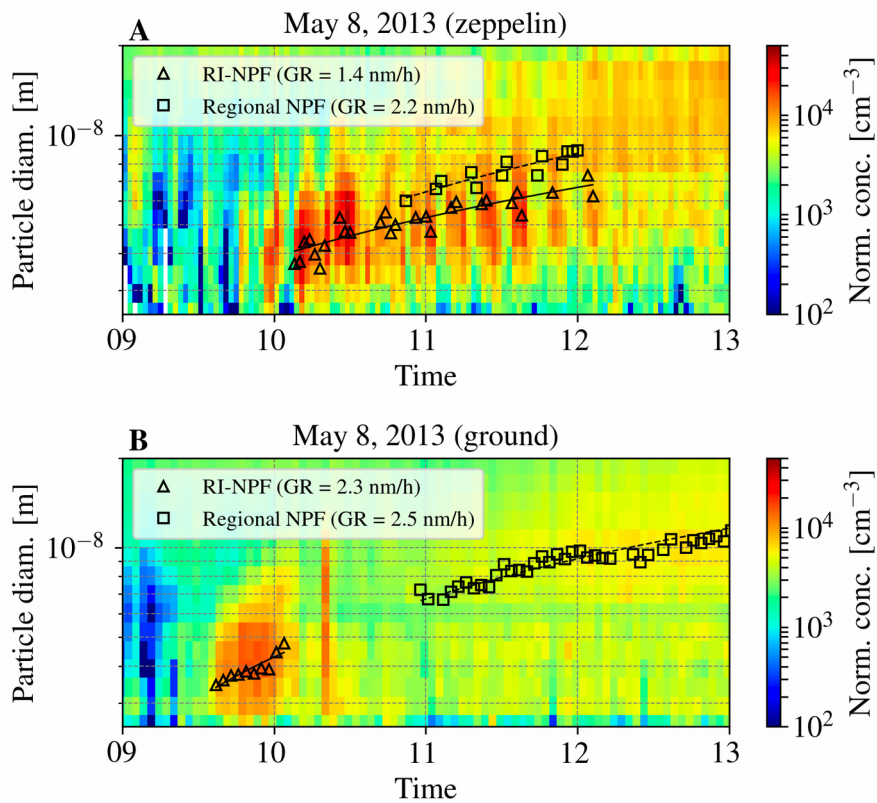
Figure 11: The particle number-size distribution (positive polarity) between 2.5-20 nm measured by the NAIS (A) on board the zeppelin and (B) at the field station on May 8, 2013. Between 10-12 the zeppelin consecutively flew through the roll-induced NPF (RI-NPF) event, leaving concentrated "stripes" on the particle number-size distribution. Between 9:30-10:00 the roll-induced NPF event moved over the field station. The black triangles and squares show the fitted mean mode diameters to the roll-induced and regional NPF event particles, respectively. Figure 8B shows simultaneous observations from the airplane. The roll-induced NPF event was moving over the measurement area from southwest to northeast. Weather radar observations showed that rolls were present over the measurement site and power spectra of the wind components from the station's mast showed that the rolls were moving over the site at the same rate (one roll in ~20 min), and in the same direction as the roll-induced NPF..
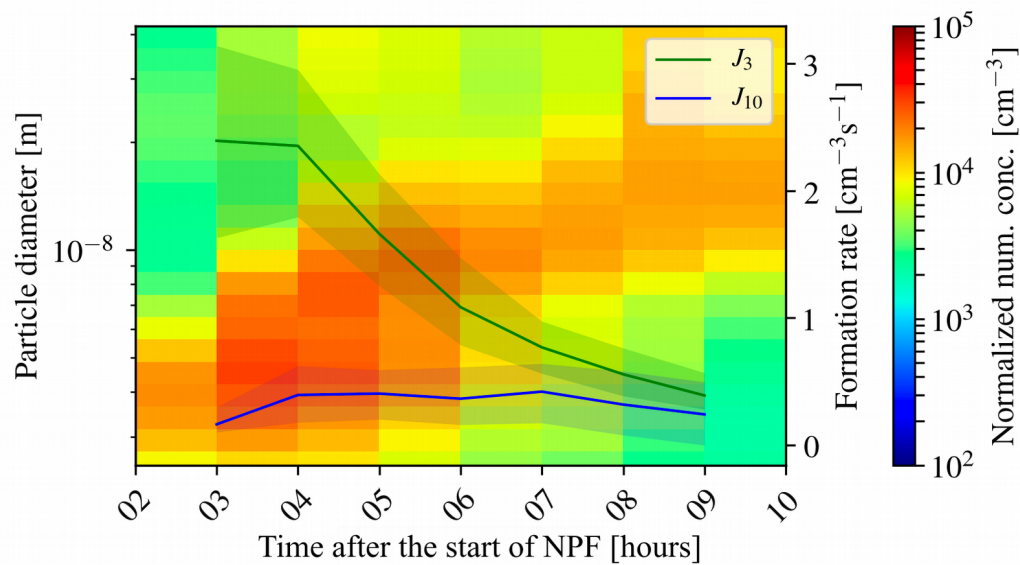
Figure 12: The above particle number-size distribution was constructed using the SMEAR II station's NAIS data by taking the roll-induced NPF observations (29 days and 46 different roll-induced NPF events) and distributing them along the time axis according to their geometric mean diameter while assuming a growth rate of 1.9 nm/h (median of the obtained GRs) and start of the NPF at t=0 hours. We used random sampling to estimate the median and the 25th and 75th percentile values for the formation rates of 3- and 10-nm-sized particles.

Table 1: Summary of airborne measurement campaigns from which data was utilized in this study. PNSD = particle number-size distribution, INSD = ion number-size distribution, PNC = particle number concentration.

Time Place	Number of flight days	Measurement platform(s)	Instruments on board the aircrafts that were used in this study
May-Jun 2013 Hyytiälä, Finland	26	Zeppelin NT Cessna 172	**Zeppelin NT** • NAIS: 2-42 nm PNSD and 0.8-42 nm positive and negative INSD • Meteorological sensors: static pressure, temperature and relative humidity **Cessna 172** • UCPC (TSI 3776 CPC): >3 nm PNC • SMPS: 10-400 nm PNSD • Li-Cor Li-840: CO_2 and H_2O vapor concentration • Meteorological sensors: static pressure, temperature and relative humidity **Cessna 172 (Aug 2015, last half of the campaign)** • AIMMS-20: 3d wind vector
Mar-Apr 2014 Hyytiälä, Finland	12	Cessna 172	
May-Jun 2014 Hyytiälä, Finland	5	Cessna 172	
Aug-Sept 2014, Hyytiälä, Finland	6	Cessna 172	
May-Jun 2015 Hyytiälä, Finland	7	Cessna 172	
Aug 2015 Hyytiälä, Finland	9	Cessna 172	

445